Cerium phosphate nanotubes: synthesis, characterization and biosensing

2009 Nanotechnology 20 035502

(http://iopscience.iop.org/0957-4484/20/3/035502)

Nanotechnology **20** (2009) 035502 (8pp) doi:10.1088/0957-4484/20/3/035502

Cerium phosphate nanotubes: synthesis, characterization and biosensing

Ling Meng, Lige Yang, Bo Zhou and Chenxin Cai[1]

Jiangsu Key Laboratory of Biofunctional Materials, College of Chemistry and Environmental Science, Nanjing Normal University, Nanjing 210097, People's Republic of China

E-mail: cxcai@njnu.edu.cn and chenxincai@hotmail.com

Received 14 September 2008, in final form 11 November 2008
Published 16 December 2008
Online at stacks.iop.org/Nano/20/035502

Abstract

Cerium phosphate (CeP) nanotubes have been synthesized and confirmed by x-ray diffraction (XRD) and transmission electron microscopy (TEM). The 1D nanomaterial has a monoclinic crystal structure with a mean width of 15–20 nm and a length up to several micrometers. The nanotubes have been employed as electrode substrates for immobilization and direct electrochemistry of heme proteins/enzymes with myoglobin (Mb) as a model. The electrochemical characteristics of the Mb–CeP/GC electrode were studied by voltammetry. After being immobilized on the nanotubes, Mb can keep its natural structure and undergo effective direct electron transfer reaction with a pair of well-defined redox peaks at $-(367 \pm 3)$ mV (pH 7.5). The apparent electron transfer rate constant is (9.1 ± 1.4) s^{-1}. The electrode displays good features in the electrocatalytic reduction of H_2O_2, and thus can be used as a biosensor for detecting the substrate with a low detection limit (0.5 ± 0.05 μM), a wide linear range (0.01–2 mM), high sensitivity (14.4 ± 1.2 μA mM^{-1}), as well as good stability and reproducibility. CeP nanotubes can become a simple and effective biosensing platform for the integration of heme proteins/enzymes and electrodes, which can provide analytical access to a large group of enzymes for a wide range of bioelectrochemical applications.

1. Introduction

Nanostructured materials have attracted much interest because they show physical properties that are significantly different from their bulk materials [1, 2]. A lot of one-dimensional (1D) nanomaterials, such as nanotubes, nanowires, nanobelts, nanorods, etc, have been prepared and extensively investigated during the past few decades because of their potential technological applications [3–8]. 1D inorganic nanomaterials have recently received much attention because they play an important role as active components or interconnects in fabricating nanoscale electronic, optical, optoelectronic, electrochemical and electromechanical devices [9–11].

Among various inorganic nanomaterials, lanthanide phosphates are of particular importance because they are widely utilized as nonlinear optical materials, phosphors, heat-resistant materials and biocompatible materials [7, 8, 12]. A particular emphasis has been placed on the study of cerium phosphate nanomaterials for applications in photonic devices [9–11]. This interest is primarily attributed to the fact that the Ce^{3+} ion exhibits a 4f–5d emission with a larger absorption in the UV region and a shorter luminescence lifetime due to allowing electric dipole transitions [13]. Although many papers have been published on the synthesis of cerium phosphate nanowires and their optical properties, studies of employing cerium phosphate as an electrode material and a protein immobilization matrix are unavailable. In our previous work, the hexagonal cerium phosphate (CeP) nanotubes were synthesized and characterized [14]. To continue exploiting the new application of CeP nanotubes, this work reports the synthesis of monoclinic structured CeP nanotubes and their use in immobilization and biosensing of heme proteins/enzymes employing myoglobin (Mb) as a model.

Mb, which functions physiologically in the storage and transport of molecular oxygen in cells, is a small heme protein found in muscle cells with a molecular weight ranging from 16 900 to 17 800 and is composed of one polypeptide chain. It is an ideal model molecule for studying the direct electron transfer (DET) reaction of heme proteins/enzymes because of its commercial availability and well-known and documented

[1] Author to whom any correspondence should be addressed.

structure. Electron transfer between Mb in solution and a bare solid electrode is usually very slow, and the electrochemical behavior is unstable and very sensitive to the sample purity and the history of the electrode surface [15]. Numerous efforts have been made to enhance the DET kinetics of Mb by using mediators, promoters or other special materials to modify the surface of the electrode [16–20]. Among these, surfactant micelles have been shown to be efficient in promoting the DET of Mb [16]. However, recent studies indicated that the surfactant had drastic effects on the structure of heme proteins and thereby led to denaturation of these proteins [21]. Therefore, it is still necessary to find new materials and simple ways to immobilize Mb, obtain its effective DET and develop an Mb-modified electrode for use in biosensors and/or in other electrochemical devices. A conventional way is to fabricate nanomaterial-based electrodes that can improve the electron transfer kinetics of redox proteins/enzymes. Among the nanomaterials used to immobilize Mb, inorganic nanomaterials are very attractive because of their chemical and thermal stability, good mechanical strength, biocompatibility and their potential for improving the stability of the proteins under extreme conditions [19, 20, 22, 23]. Here, the CeP nanotubes are used for the realization of DET between Mb and the electrode. The characteristics of the DET and electrocatalytic features of the immobilized Mb are presented. To the best of our knowledge, this is the first example that uses rare-earth metal phosphate nanotubes as a new electrode material in facilitating DET between biomolecules and an electrode.

2. Experimental details

2.1. Chemicals

Mb (from horse skeletal muscle, type III, Sigma) was used without further purification. Solutions of H_2O_2 were freshly diluted from the 30% solution and their concentrations were determined using a standard solution of $KMnO_4$. All the other chemicals were of analytical grade and used as received. 0.1 M phosphate buffer solutions (PBS, pH 7.5) were employed as the supporting electrolyte.

2.2. Preparation of CeP nanotubes

CeP nanotubes were synthesized via the hydrothermal method, which has been regarded as an effective route to fabricate high-quality anisotropic nanomaterials [24]. In the typical synthesis of CeP nanotubes, 25 ml of Na_3PO_4 solution (0.8 M) was added to 25 ml of $Ce(NO_3)_3$ solution (0.8 M) under vigorous stirring. Then the pH value of the solution was adjusted to below 1 using 0.1 M HCl under stirring. After that, the solution was transferred to a Teflon-lined autoclave until approx. 80% of the autoclave capacity was filled. After being sealed, the autoclave was maintained at 200 °C for 8 h and then allowed to naturally cool to room temperature. Subsequently, CeP nanotubes were collected by filtering. The sample was washed thrice with distilled water and absolute ethanol, and vacuum-dried at room temperature.

2.3. Immobilization of Mb and fabrication of the Mb–CeP/GC electrode

Several parameters were optimized to obtain the best voltammetric response. For the immobilization of Mb, 20 mg of CeP nanotubes was dispersed in 4 ml Mb solution (2 mg ml^{-1}, in PBS, pH 7.5) and the mixture was stirred at 4 °C overnight. During this period Mb was spontaneously adsorbed on the surface of CeP nanotubes. The resulting Mb–CeP composite was collected by centrifugation and washed with water to remove those loosely adsorbed Mb molecules.

For the preparation of the modified electrode, 10 mg of the Mb–CeP composite was suspended in 0.5 ml of PBS (pH 7.5) and 2 μl of the suspension was deposited onto the surface of the GC electrode (GC, 3 mm in diameter, CH Instruments), which was treated following the procedures reported previously [25]. The solvent was allowed to evaporate before use. The resulting electrode was denoted as the Mb–CeP/GC electrode, and stored at 4 °C when not in use.

Using similar procedures, the CeP/GC and Mb/GC electrodes were also fabricated. Their electrocatalytic characteristics were compared with that of the Mb–CeP/GC electrode.

2.4. Apparatus

X-ray powder diffraction (XRD) patterns of CeP nanotubes were recorded on a Rigaku/Max-3A x-ray diffractometer with Cu Kα radiation (λ = 0.154 18 nm). The operational voltage and current were maintained at 40 kV and 40 mA, respectively. Scanning electron microscopic (SEM) images of CeP and Mb–CeP on the surface of the GC electrode were recorded using a JEOL JSM-5610LV scanning electron microscope (Japan). Transmission electron microscopic (TEM) images were obtained on a JEOL-2010 microscope with an accelerating voltage of 200 kV. Energy-dispersive x-ray spectroscopy (EDS) was obtained from an attached Oxford Link ISIS energy-dispersive spectrometer fixed to the microscope. The sample was prepared by sonicating CeP nanotubes in ethanol for 20 min and evaporating one drop of the suspension onto a carbon-coated holey film supported on a copper grid for TEM measurements. UV–vis spectra were recorded using a Cary 5000 UV–vis–NIR spectrophotometer (Varian, USA) by dispersing CeP or Mb–CeP in aqueous solution (both at a level of 2 mg ml^{-1}). For comparison, the UV–vis spectrum of Mb aqueous solution (0.5 mg ml^{-1}) was also recorded. Circular dichroic (CD) measurements were made on a JASCO Model J-810 dichrograph (Japan Spectroscopic Co. Ltd, Japan) in a 1 cm quartz cuvette. The final spectra were the mean of ten accumulated scans, and were corrected for the unspecific dichroic absorbance of the medium by computer manipulation.

The electrochemical experiments were performed with a CHI 660B electrochemical workstation (CH Instruments). The coiled Pt wire and the saturated calomel electrode (SCE) were used as the counter electrode and the reference electrode, respectively. Buffers were purged with high purity nitrogen for at least 30 min prior to experiments and the nitrogen environment was then kept over the solution to prevent it from

oxygenation. All electrochemical experiments were performed at room temperature (22 ± 2 °C).

3. Results and discussion

3.1. Characterization of CeP nanotubes

TEM images show that the synthesized CeP samples are composed of well-defined rigid nanotubes, and these nanotubes are straight and highly uniform in morphology (figure 1(A)). The hollow along the center of the tube is clear and the open end of the nanotubes can also be seen clearly (figure 1(B)). The nanotubes have a mean width of 15–20 nm and a length up to several micrometers, and thus the aspect ratio is high. The EDS was recorded to verify the composition of as-synthesized CeP nanotubes. The results shown in figure 1(C) reveal the presence of cerium (4.82, 5.24, 5.60 keV), phosphorus (2.01 keV), oxygen (0.52 keV) and carbon (0.27 keV). The amount of carbon is very little (only 1.2% in atomic ratio). Cerium and phosphorus are observed with an estimated atomic ratio of 1:1 (16.5:16.6), indicating the CeP nanotubes have the stoichiometric formula of $CePO_4$. This result is in good agreement with that expected by theory.

The CeP nanotubes were also examined by XRD measurements as shown in figure 1(D). All the XRD patterns in figure 1(D) can be readily indexed to a pure monoclinic phase of $CePO_4$ with lattice constants highly comparable to the values from the JCPDS card (JCPDS 32-0199). No impurity phases could be found from the XRD patterns of the synthesized products. The well-defined peaks indicate that CeP nanotubes are crystalline.

SEM images can provide information on the morphologies of CeP nanotubes and Mb–CeP on the surface of the GC electrode. The image of the CeP indicates that the nanotubes distribute almost uniformly on the entire surface of the GC electrode, exhibiting a special three-dimensional structure (figure 2(a)). The uniform nanostructure can significantly increase the effective surface of the electrode for loading biomolecules. The morphology of Mb–CeP presented in figure 2(b) shows that the size of Mb–CeP bundles is slightly larger than that of CeP nanotubes, indicating the immobilization of Mb on the surface of CeP nanotubes. Moreover, the morphology of Mb–CeP on the electrode surface possesses the similar three-dimensional structure to that of CeP nanotubes. Such a structure is expected to be very attractive for the detection of substrates because each of the Mb–CeP composites is fully and easily accessible to substrates, and thus can be used as an electrochemical sensing unit, yielding a high signal-to-noise ratio for electrochemical determination.

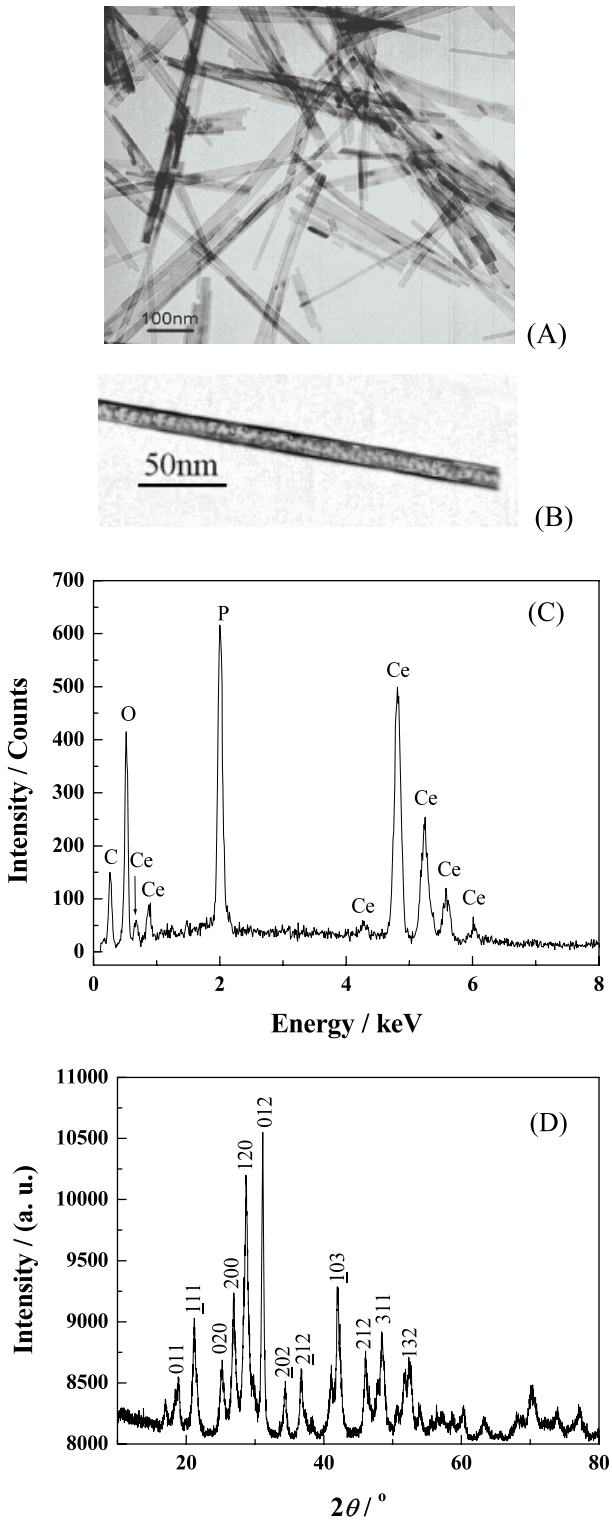

Figure 1. (A) TEM image of CeP nanotubes. (B) TEM of a single CeP nanotube. (C) The EDS spectrum of CeP nanotubes. (D) X-ray diffraction patterns of CeP nanotubes.

3.2. UV–vis and CD spectra characterization

UV–vis spectroscopy is a useful tool for monitoring the possible change of the Soret absorption band of the heme group. The bandshift provides information on the possible denaturation of heme proteins, particularly conformational changes of these proteins [26]. The UV–vis spectrum of CeP nanotubes shows four peaks at 215, 236, 258 and 275 nm, respectively (figure 3(a)). These peaks correspond to theoretical values (203–276 nm) of Ce^{3+} ion f–d electron transitions from the $4f^1$ ground state to the five $5d^1$ levels split within a monoclinic crystal field [27]. The absorption characteristics are in good agreement with those for f–d electron transitions in $CePO_4$ bulk materials [27] and cerium phosphate nanowires [11],

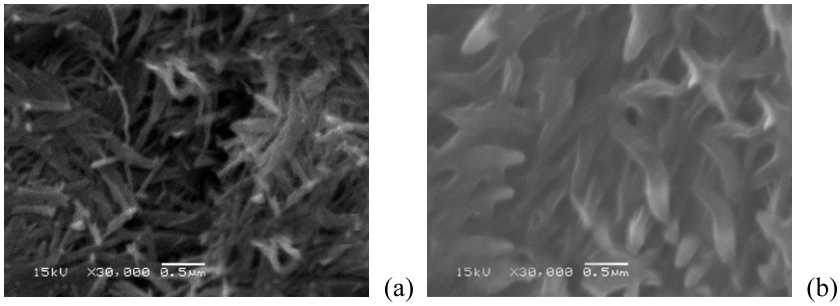

Figure 2. Typical SEM images of CeP nanotubes (a) and Mb–CeP (b) on the surface of GC electrode.

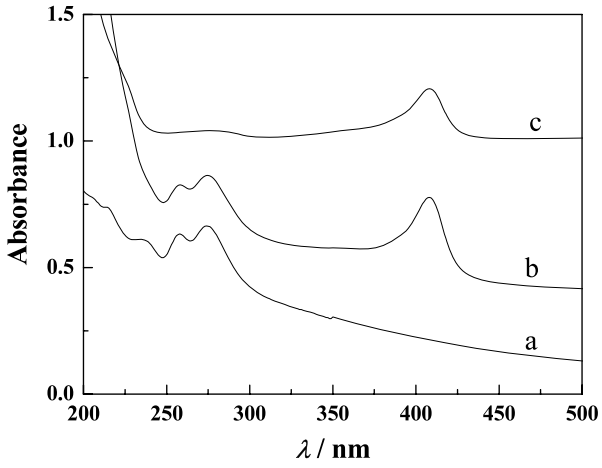

Figure 3. UV–vis spectra of CeP nanotubes (a), Mb–CeP (b) and Mb in aqueous solution (0.5 mg ml^{-1}, (c)).

indicating that useful optical properties are retained in the CeP nanotubes synthesized in this work.

The UV–vis spectrum of Mb–CeP is depicted in figure 3(b). In this spectrum, the absorption peaks of CeP nanotubes appear at 258 and 275 nm, which are the same as those in figure 3(a). The other two absorption peaks of CeP nanotubes (215 and 236 nm) cannot be detected from figure 3(b) due to the steep rise in absorbance at the wavelength below 250 nm (figure 3(b)). The peak at 408 nm in figure 3(b) is attributed to the Soret band of the immobilized Mb, indicating the successful immobilization of Mb on CeP nanotubes. The features of this peak are identical with those of natural Mb dissolving in solution (408 nm, figure 3(c)), suggesting no significant denaturation occurred to the protein after immobilized onto the CeP nanotubes' surface. These results also show good biocompatibility of CeP nanotubes.

CD spectroscopy is also used to characterize the structural integrity of Mb immobilized on CeP nanotubes since it is able to give an insight into the structure and the conformation of proteins/enzymes [28]. The spectrum in the far-UV region (200–250 nm) corresponds to the peptide $n \rightarrow \pi^*$ electronic transition and it is sensitive to the conformational changes of proteins. The spectra of Mb aqueous solution in this region exhibited two negative peaks at approx. 208 and 223 nm (figure 4(a)), respectively. The characteristics are similar to those of the other heme protein [29]. The CD spectrum

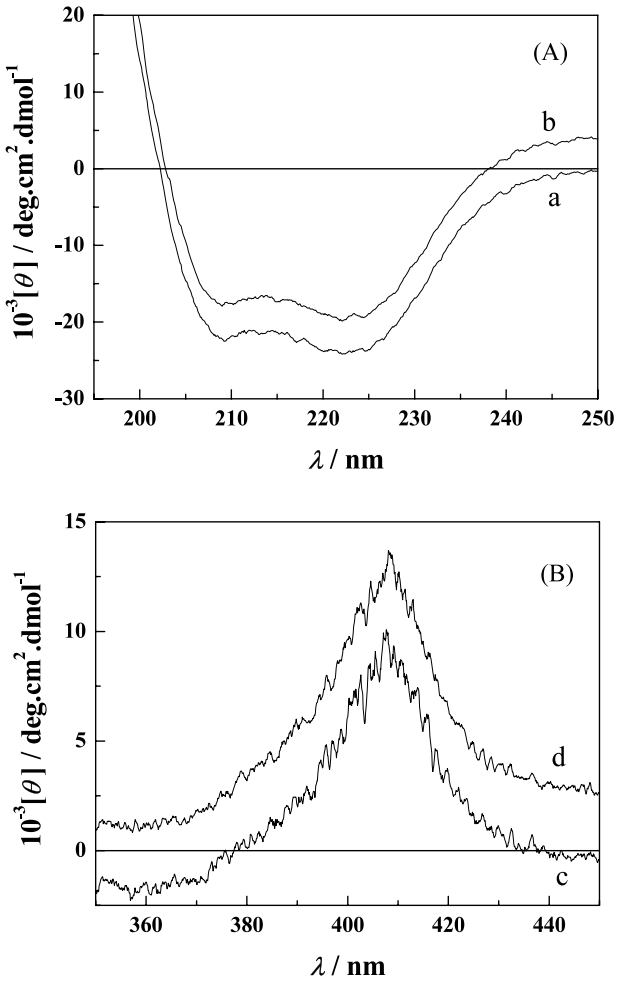

Figure 4. (A) Far-UV CD spectra of Mb aqueous solution (a) and Mb–CeP (b). (B) Soret CD spectra of Mb aqueous solution (c) and Mb–CeP (d). Curves (b) and (d) are displayed shifted by four units for clarity.

of Mb–CeP (figure 4(b)) in this region is also characterized by two negative peaks, whose positions are almost the same as those in figure 4(a), indicating that the structure and the conformation of Mb after being confined on the surface of CeP nanotubes are essentially the same as those in its natural state. Moreover, the CD spectra of Mb–CeP (figure 4(d)) in the near-UV region (250–300 nm) are also similar to those of the Mb aqueous solution (figure 4(c)). These results verify that the

microenvironment of the active site of the protein in Mb–CeP also remains the same as that of the native one since no signals can be observed in this region for a denatured protein [29]. The result is in good agreement with that obtained from UV–vis spectra.

3.3. DET of Mb

The cyclic voltammograms of CeP/GC (a), Mb–CeP/GC (b) and Mb/GC (c) electrodes in 0.1 M of PBS (pH 7.5) are depicted in figure 5. No redox peaks are observed at the CeP/GC electrode in the potential range of interest (curve (a)), indicating that CeP nanotubes are inelectroactive. The cyclic voltammogram of the Mb/GC electrode shows a small cathodic peak at approx. −390 mV and the anodic peak is undetectable (curve (c)). Moreover, the height of the cathodic peak decreases rapidly and the peak disappears completely within a few scanning cycles (approx. 3–5 cycles). These suggest that Mb cannot undergo the effective DET reaction at the surface of the bare GC electrode due to the redox center being deeply buried in the interior of the molecule.

Curve (b) in figure 5 shows a pair of well-defined and nearly symmetrical redox peaks at the Mb–CeP/GC electrode with the anodic and cathodic peak potentials at −350 and −385 mV (at 100 mV s^{-1}), respectively. This pair of peaks is ascribed to the DET reaction (the conversion of Fe(III)/Fe(II) center) of Mb immobilized on the surface of CeP nanotubes. The separation of peak potentials, ΔE_p, is 35 mV, indicating that Mb on CeP nanotubes can display a quasi-reversible electrochemical reaction despite its large molecular structure. Its formal potential, $E^{0'}$, which is defined as the average of anodic and cathodic peak potentials, is −367.5 mV (at 100 mV s^{-1}). The value of $E^{0'}$ is close to that previously reported for Mb trapped in polymer films, such as polyacrylamide (−335 mV) [30] or Eastman AQ film (−362 mV) [31], and also similar to those obtained by adsorbing Mb on the surface of clay (−330 mV) [18] and carbon nanotubes (370 mV) [20]. Moreover, it is also similar to those of other heme proteins (enzymes) including hemoglobin [32] and horseradish peroxidase [33, 34]. These show that CeP nanotubes can facilitate the effective DET between Mb and the electrode surface, and moreover Mb immobilized on the surface of CeP nanotubes can keep its natural structure. The conclusion is in good agreement with that obtained from UV–vis and CD spectra. Furthermore, the Mb–CeP on the GC electrode surface is fairly stable since the features of the cyclic voltammogram of the Mb–CeP/GC electrode remain unchangeable after the electrode was scanned continuously for a long time (∼100 cycles, at 50 mV s^{-1}) in the potential range of interest. In addition, no obvious change is detected after the electrode has been stored in PBS at 4 °C for one week. These characteristics are important when the electrode is further used as a biosensor for sensing substrates (such as H_2O_2, etc). The good stability of the Mb–CeP/GC electrode is due to that Mb–CeP can form a thin and uniform film on the surface of the GC electrode (figure 2(b)). This kind of film does not leak from the electrode surface and can stably adhere on the GC surface for a long time. The experimental results indicate that a thick film of Mb–CeP on the electrode surface is not stable and is easy to split from the electrode surface. For example, if the amount of Mb–CeP suspension added to the GC electrode surface is increased to 10 μl, this thick film leaks from the electrode surface within 10 scanning cycles.

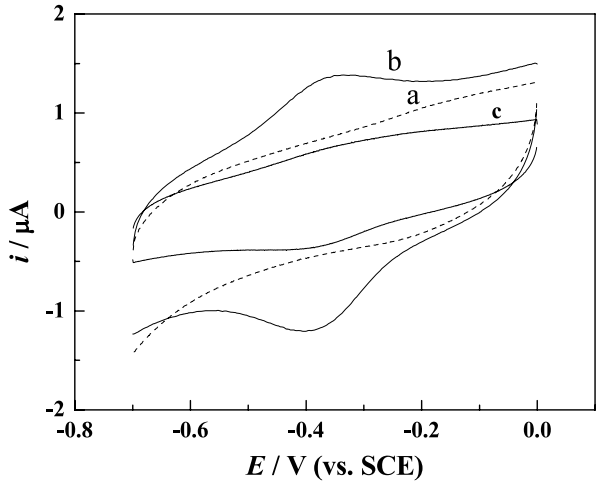

Figure 5. Cyclic voltammograms of the CeP/GC (a), Mb–CeP/GC (b) and Mb/GC (c) electrode in 0.1 M of PBS (pH 7.5) at a scan rate of 100 mV s^{-1}.

To further investigate the characteristics of Mb adsorbed on the surface of CeP nanotubes, the effects of scan rate on the voltammetric response of the Mb–CeP/GC electrode was studied in detail (figure 6). From figure 6(A), almost equal cathodic and anodic peak heights can be observed at each scan rate, indicating that all electroactive ferrous Mb (Mb–Fe(II)), which was produced by reduction of ferric Mb (Mb–Fe(III)) on the forward scan, can be oxidized to Mb–Fe(III) on the reverse scan. Both the anodic and cathodic peak currents increase linearly with the scan rate up to at least 1000 mV s^{-1} (figure 6(B)), which suggests that the redox process is confined to the surface of the electrode, also confirming that the immobilized state of Mb is stable. Although the anodic and cathodic peak potentials shift slightly to more positive and negative potentials, respectively, with the increase of the scan rate, the values of $E^{0'}$ (the average value is $-(367 \pm 3)$ mV in the scan rate range from 50 to 1000 mV s^{-1}) are almost independent of the scan rates. From the dependence of ΔE_p on the scan rate, the apparent heterogeneous electron transfer rate constant, k_s, can be calculated to be (9.1 ± 1.4) s^{-1}, using the method developed by Laviron [35] for a surface-controlled electrochemical system. This value is comparable to that obtained by entrapping Mb within the bicontinuous gyroidal mesoporous carbon (BGMC) matrix (10.4 s^{-1}) [36], and is much higher than those reported previously by adsorbing Mb on the surface of carbon nanotubes (3.11 ± 0.98 s^{-1}) [20] and bioconjugating Mb with porous nanogranules of zirconium uridine monophosphate, $Zr(UMP)_2 \cdot H_2O$, (1.1 ± 0.3 s^{-1}) [37]. These results indicate that CeP nanotubes can facilitate DET between the adsorbed protein and the electrode surface more effectively.

The surface coverage (Γ) of Mb on the surface of CeP nanotubes can be determined by integrating the anodic or

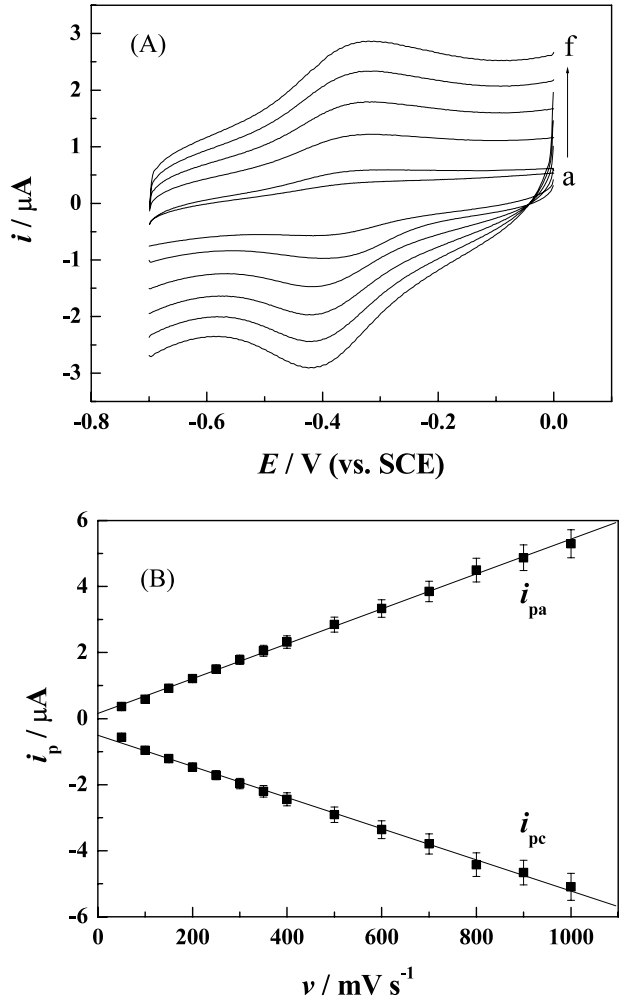

Figure 6. (A) Cyclic voltammograms of the Mb–CeP/GC electrode at scan rates of (from (a) to (f)) 50, 100, 200, 300, 400 and 500 mV s^{-1}, respectively. (B) The dependence of anodic (i_{pa}) and cathodic (i_{pc}) peak current on the scan rates.

cathodic peak in cyclic voltammograms using the equation $Q = nFA\Gamma$, where Q is the charge involved in the reaction, n is the number of electrons transferred, F is Faraday's constant and A is the apparent area of the electrode, which was estimated using the method reported previously [32]. This procedure generates the Γ of $(3.63 \pm 0.69) \times 10^{-11}$ mol cm^{-2}. The value is close to the theoretical one for monolayer coverage of Mb (1.38×10^{-11} mol cm^{-2}). The theoretical value was calculated from the crystallographic dimensional structure of Mb (approx. 3 nm × 4 nm × 5 nm) [38] assuming that the molecule adopts an orientation with the long axis parallel to the electrode surface [7].

3.4. Effects of solution pH

It has been reported that solution pH modulates the accessibility of water molecules to the heme pocket and the protonation of the heme iron-bound histidine in heme proteins, and thus affecting the redox potential of these proteins [39]. Cyclic voltammetric characteristics of the Mb–CeP/GC electrode show a considerable dependence on

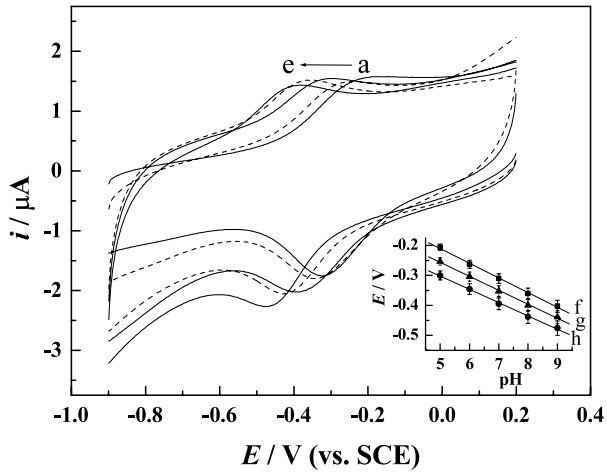

Figure 7. Cyclic voltammograms of the Mb–CeP/GC electrode in 0.1 M of PBS at pHs of (a) 5.0, (b) 6.0, (c) 7.0, (d) 8.0 and (e) 9.0. The scan rate is 100 mV s^{-1}. The inset shows the dependence of E_{pa} (f), E_{pc} (h) and $E^{0'}$ (g) on the solution pH.

pH of the buffer. An increase of pH in solution leads to a negative shift in potential of both the anodic and cathodic peaks (figures 7(a)–(e)). The inset of figure 7 shows the dependence of E_{pa}, E_{pc} and $E^{0'}$ of the Mb–CeP/GC electrode on the solution pH. All the E_{pa}, E_{pc} and $E^{0'}$ have a linear relationship with solution pH with a slope of −49, −45 and −47 mV pH^{-1} units, respectively, in the range of 5.0–9.0. The values are very close to those obtained by Li *et al* at the $\{clay/Mb\}_6$ electrode (−42.4 mV pH^{-1}) [18], Cao *et al* at gold nanoparticles/carbon nanotubes nanohybrid film electrode (42.2 mV pH^{-1}) [40] and Lü *et al* at the carbon nanotubes' electrode (−43.7 mV pH^{-1}) [20]. However, they are quite different from the theoretical value of −58.6 mV pH^{-1} at 22 °C for a reversible electron transfer reaction coupled with an equal number of protons and electrons. The reason that causes this difference cannot yet be fully understood at present, but it has probably resulted from the influence of the protonation states of amino acids near the heme and protonation of the water molecules coordinated to the heme iron [41]. This influence leads to more complex reaction mechanisms of the electron transfer process between the electrode and the protein, in which the ratio of the number of protons to the number of electrons is more complicated. The microenvironment of Mb at the surface of the electrode may significantly influence the detailed mechanism of the DET of the protein. The overall reaction of DET of Mb at CeP nanotubes may include several fundamental steps, and some steps correspond to the transfer of one or more protons. Thus, it is not surprising that the total number of electrons and protons involved in the overall reaction is not equal. Nevertheless, the pH-dependent peak potential in figure 7 indicates that the electron transfer between the protein and the electrode is indeed accompanied by proton transfer.

3.5. Electrocatalysis of Mb–CeP/GC electrode

It was reported that heme proteins (enzymes), such as cytochrome *c*, hemoglobin, Mb, etc, usually have good

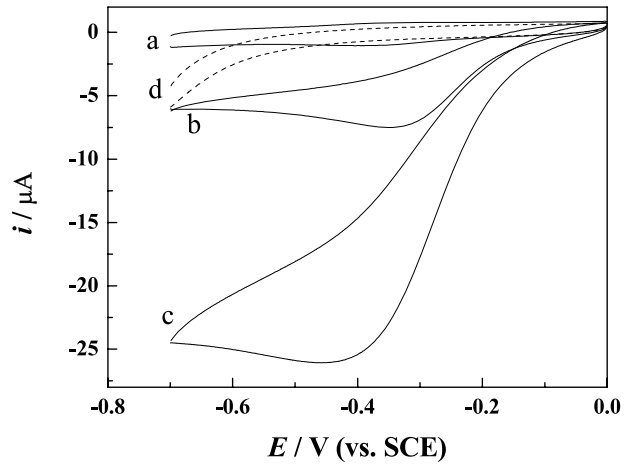

Figure 8. Electrocatalytic responses of the Mb–CeP/GC electrode towards the reduction of O_2 in N_2-saturated (a), air-saturated (b) and O_2-saturated (c) PBS (pH 7.5). Curve (d) is the voltammetric response of the CeP/GC electrode in air-saturated PBS. Scan rate is 100 mV s^{-1}.

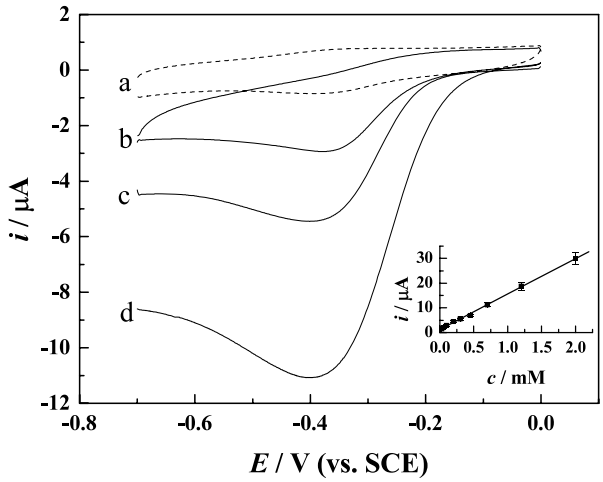

Figure 9. Voltammetric responses of Mb–CeP/GC electrode in PBS (pH 7.5) in the absence (a) and presence of 0.1 (b), 0.3 (c) and 0.7 mM H_2O_2 (d). Scan rate is 100 mV s^{-1}. The inset shows dependence of i_{cat} on the concentration of H_2O_2.

electrocatalytic activities toward the reduction of O_2, trichloroacetic acid, H_2O_2, etc [25, 42]. Having demonstrated the DET characteristics of the Mb–CeP/GC electrode, we next study the bioelectrocatalytic activities of the electrode towards the reduction of H_2O_2 and O_2. Figures 8(a) and (b) demonstrate the cyclic voltammograms of the Mb–CeP/GC electrode obtained in N_2-saturated (figure 8(a)) and air-saturated (figure 8(b)) PBS (pH 7.5), respectively. Compared with figure 8(a), the shape of the cyclic voltammogram of the electrode in the air-saturated solution changes significantly and is characterized by a large cathodic peak at approx. −340 mV (figure 8(b)). The anodic peak disappears completely. The onset potential (at approx. −30 mV) is 310 mV more positive than the reduction peak actually appears. The results indicate that the Mb at the surface of CeP nanotubes retains its electrocatalytic activity to the reduction of O_2. The electrocatalytic current increases significantly when a cyclic voltammetric experiment is performed in O_2-saturated PBS (figure 8(c)). The controlled experimental results show that the CeP/GC electrode has a very low electrocatalytic activity toward the reduction of O_2 only at the potential below −550 mV (figure 8(d)), suggesting that the reduction of O_2 in figures 8(b) and (c) mainly comes from the electrocatalysis of Mb.

The electrocatalytic reduction of H_2O_2 was also studied at the Mb–CeP/GC electrode by cyclic voltammetry, as shown in figure 9. In the absence of H_2O_2, a pair of redox peaks of Mb is observed (figure 9(a)). However, in the presence of 0.1 mM of H_2O_2, the voltammetric behavior changes drastically. A large cathodic current of the reduction of H_2O_2 appears at approx. −360 mV and the anodic peak completely disappears (figure 9(b)). The onset potential (at approx. −160 mV) is 200 mV more positive than the reduction peak actually appears. The electrocatalytic cathodic currents are enhanced significantly by a further increase of the concentration of H_2O_2 in the solution (figures 9(c) and (d). For clarity, the reversed voltammetric curves of figures 9(c) and (d) are omitted.) The electrocatalytic current is linear within the concentration of H_2O_2 from 0.01 to 2 mM with a detection limit of approx. (0.5 ± 0.05) μM (inset in figure 9). The sensitivity is calculated to be (14.4 ± 1.2) μA mM^{-1}. The linear response range is wider than those of 4–124, 2–500, 3.92–180.14, 24.2–167, 1–42 and 2–160 μM reported previously by immobilizing Mb at a hexagonal mesoporous silica matrix [19], at a gold nanoparticles/carbon nanotubes nanohybrid film [40], at a porous nanogranule of $Zr(UMP)_2{\cdot}H_2O$ [37], at single-walled carbon nanotubes (SWCNTs)–cetyltrimethylammonium bromide (CTAB) nanocomposite [43], at TiO_2-coated multi-walled carbon nanotubes (MWCNTs) [44] and at titanate nanotubes [45], respectively. The value of the detection limit obtained in this work is similar to that acquired at titanate nanotubes (0.6 μM) [45] and at the TiO_2-MWCNT nanocomposite (0.41 μM) [44], and is much lower than 1.52 and 8.07 μM reported for the conjugation film of the Mb–$Zr(UMP)_2{\cdot}H_2O$ [37] and SWCNTs-CTAB [43], respectively. The sensitivity obtained in the present case is also comparable to that reported for TiO_2-MWCNT nanocomposites (17.52 nA μA^{-1}) [44]. Therefore, it can be concluded that Mb–CeP presents a good analytical performance in the determination of H_2O_2.

All these features, along with electrocatalytic characteristics of the reduction of O_2, indicate that Mb immobilized on the CeP nanotubes keeps intrinsic and good electrocatalytic activities towards its substrates. The biocompatibility of CeP nanotubes enables the nanomaterial to become a good biosensing platform for realizing direct electrochemistry and electrocatalysis of heme-containing proteins/enzymes.

3.6. Reproducibility and stability

Additional experiments were conducted to test the reproducibility and stability of the Mb–CeP/GC electrode toward the reduction of H_2O_2. Five different and freshly prepared electrodes were employed to detect the reduction of H_2O_2

in concentrations of 0.01–2 mM. The RSD (relative standard deviation) is 2.4% estimated from the slopes of five calibration curves (a calibration curve for each electrode). The assay precision of the electrode was examined by ten determinations at a H_2O_2 concentration of 0.1 mM. An RSD of 3.2% is obtained. These reveal an acceptable reproducibility and precision in the construction of the electrode. No obvious change in the response is found after the electrode was immersed in solution and stored at 4 °C for 10 h. The response of the electrode to 0.1 mM H_2O_2 can keep 95% of its initial one within two weeks. These results on stability can be, in general, advantageously compared with those reported for the carbon-nanotube-based biosensors [43, 44]. For example, the response current at the Mb-SWCNT-CTAB film electrode retained only 78% of the initial response after the electrode was stored for about two weeks [43]. The higher stability can be attributed to the capability of the CeP nanotubes immobilizing Mb molecules and retaining their biological activities. This improved stability may also be attributed to the special three-dimensional structure of the Mb–CeP (figure 2(b)), which is beneficial for the substrates getting access to the enzyme molecules. These results indicate that the stability of the electrode is acceptable.

4. Conclusions

Cerium phosphate (CeP) nanotubes have been synthesized by a facile hydrothermal method and characterized using TEM and XRD. The resulting 1D nanomaterial has a monoclinic crystal structure with a high aspect ratio. The CeP nanotubes have been employed as electrode substrates for immobilization and direct electrochemistry of heme proteins, Mb. The electrochemical characteristics of the Mb–CeP/GC electrode were studied by voltammetry. After being immobilized on the surface of CeP nanotubes, Mb can still retain its natural structure and undergo effective direct electron transfer reaction with a pair of well-defined, quasi-reversible redox peaks in its cyclic voltammogram. The electrode displays good features in the electrocatalytic reduction of oxygen and hydrogen peroxide, and thus can be used as a biosensor for detecting substrates with good reproducibility and stability.

Acknowledgments

This work is supported by the National Natural Science Foundation of China (20673057, 20773067 and 20833006), the Program for New Century Excellent Talents in University (NET-06-0508) and the Foundation of the Jiangsu Education Committee (06KJB150061).

References

[1] Lee K J, Oh J H, Kim Y and Jang J 2006 *Chem. Mater.* **18** 5002
[2] Liu J, Li X and Dai L 2006 *Adv. Mater.* **18** 1740
[3] Xia Y, Yang P, Sun Y, Wu Y, Mayers B, Gates B, Yin Y, Kim F and Yan H 2003 *Adv. Mater.* **15** 353
[4] Liu L, Song J F, Yu P F and Cui B 2007 *Talanta* **71** 1842
[5] Shi Y, Zhou B, Wu P, Wang K and Cai C X 2007 *J. Electroanal. Chem.* **611** 1
[6] Inguanta R, Piazza S and Sunseri C 2008 *Electrochem. Commun.* **10** 506
[7] Liu Y, Zhang J, Hou W and Zhu J J 2008 *Nanotechnology* **19** 135707
[8] Zhang L 2008 *Biosens. Bioelectron.* **23** 1610
[9] Bu W, Hua Z, Chen H and Shi J 2005 *J. Phys. Chem.* B **109** 14461
[10] Tang C, Bando Y, Golberg D and Ma R 2005 *Angew. Chem. Int. Edn* **44** 576
[11] Xing Y, Li M, Davis S A and Mann S 2006 *J. Phys. Chem.* B **110** 1111
[12] Yu L, Song H, Liu Z, Yang L, Lu S and Zheng Z 2005 *J. Phys. Chem.* B **109** 11450
[13] Francini R, Grassano U M, Landi L, Scacco A, Elena M D, Nikl M, Cechova N and Zema N 1997 *Phys. Rev.* B **56** 15109
[14] Yang L G, Zhou B, Lu T H and Cai C X 2008 *Chin. J. Appl. Chem.* **25** 697
[15] Chattopadhyay K and Mazumdar S 2000 *Bioelectrochemistry* **53** 17
[16] Rusling J F 1998 *Acc. Chem. Res.* **31** 363
[17] Ma H, Hu N and Rusling J F 2000 *Langmuir* **16** 4969
[18] Li Z and Hu N 2003 *J. Electroanal. Chem.* **558** 155
[19] Dai Z, Xu X and Ju H 2004 *Anal. Biochem.* **332** 23
[20] Lü Y F, Yin Y J, Wu P and Cai C X 2007 *Acta Phys.-Chim. Sin.* **23** 5
[21] de Groot M T, Merkx M and Koper M T M 2005 *J. Am. Chem. Soc.* **127** 16224
[22] Yu X, Chattopadhyay D, Galeska I, Papadimitrakopoulos F and Rusling J F 2003 *Electrochem. Commun.* **5** 408
[23] Yu J, Zhao T, Zhao F and Zeng B 2008 *Electrochim. Acta* **53** 5760
[24] Patzke G R, Krumeich F and Nesper R 2002 *Angew. Chem. Int. Edn* **41** 2446
[25] Du P, Liu S, Wu P and Cai C X 2007 *Electrochim. Acta* **52** 6534
[26] Chi Z and Asher S A 1998 *Biochemistry* **37** 2865
[27] Nakazawa E and Shiga F 2003 *Japan. J. Appl. Phys.* 1 **42** 1642
[28] Degli Esposti M, Ballester F, Solaini G and Lenaz G 1987 *Biochem. J.* **241** 285
[29] Kawamura-Konishi Y, Kihara H and Suzuki H 1988 *Eur. J. Biochem.* **170** 589
[30] Shen L, Huang R and Hu N 2002 *Talanta* **56** 1131
[31] Hu N and Rusling J F 1997 *Langmuir* **13** 4119
[32] Cai C X and Chen J 2004 *Anal. Biochem.* **325** 285
[33] Sun D, Cai C X, Li X, Xing W and Lu T H 2004 *J. Electroanal. Chem.* **566** 415
[34] Zhao G C, Yin Z Z, Zhang L and Wei X W 2005 *Electrochem. Commun.* **7** 256
[35] Laviron E 1979 *J. Electroanal. Chem.* **101** 19
[36] You C, Yan X, Kong J, Zhao D and Liu B 2008 *Electrochem. Commun.* **10** 1864
[37] Qiao Y, Jian F and Bai Q 2008 *Biosens. Bioelectron.* **23** 1244
[38] Singh-Zocchi M, Hanne F and Zocchi G 2002 *Biophys. J.* **83** 2211
[39] Lei C, Wollenberger U, Bistolas N, Guiseppi-Elie A and Scheller F W 2002 *Anal. Bioanal. Chem.* **372** 235
[40] Cao W, Wei C, Hu J and Li Q 2008 *Electroanalysis* **20** 1925
[41] Liu H, Tian Z, Lu Z, Zhang Z, Zhang M and Pang D 2004 *Biosens. Bioelectron.* **20** 294
[42] Lu X, Hu J, Yao X, Wang Z and Li J 2006 *Biomacromolecules* **7** 975
[43] Wang S, Xie F and Liu G 2008 *Talanta* doi:10.1016/j.talanta.2008.09.019
[44] Zhang L, Tian D B and Zhu J J 2008 *Bioelectrochemistry* **74** 157
[45] Liu A H, Wei M D, Honma I and Zhou H S 2005 *Anal. Chem.* **77** 8068